



Improvements of portable energy dispersive X-ray fluorescence instrument: Resolution with Silicon Drift Detector, measurements stability using pyroelectric sources, and adaptation for space use

Alain Carapelle¹  | Gary Lejeune¹ | Mathieu Morelle²  | Olivier Evrard² | Paul Leroux³ | Jeffrey Prinzie³ | Ying Cao⁴ | Bjorn Van Bockel⁴ | Francis Montfort¹ | Nicolas Martin¹

¹Centre Spatial de Liège, Liege University, Liège, Belgium

²Mirion Technologies (Canberra Olen) NV, Olen, Belgium

³Department of Electrical Engineering (ESAT), ADVISE, KU Leuven, Leuven, Belgium

⁴MAGICS, Geel, Belgium

Correspondence

Alain Carapelle, Centre Spatial de Liège, Liege University, Liège, Belgium.

Email: a.carapelle@uliege.be

Funding information

Belgian Federal Science Policy Office

Abstract

An energy dispersive X-ray fluorescence instrument has been developed to be used for space exploration. In particular, the electronic readout has been redesigned to withstand the radiation environment of space and improve the energy resolution down to 121.17 eV using an Silicon Drift Detector (SDD). Besides, the instrument uses pyroelectric sources as excitation sources. We include a renormalization to reduce measurement fluctuation from 25.2% to 3.7%. A peak search algorithm has been implemented based on calibration to improve accuracy and reduce possible aging drift effects.

KEYWORDS

energy dispersive X-ray fluorescence, resolution, SDD, stability, space

1 | INTRODUCTION

Portable X-ray fluorescence spectrometers are used in a wide range of applications (archeometry,¹ contaminated land,^{2,3} coating thickness measurement,⁴ geology,⁵ alloy analysis and identification,⁶ etc.) and are paramount instruments for planetary science since the beginning of space exploration. Improvements in detectors and electronics allowed to improve the capabilities of such planetary instruments.⁷ Up to now, all these space instruments have used radioisotopes sources as excitation sources. The only exception is the very last PIXL instrument⁸ sent on Mars by NASA onboard Perseverance, which uses an X-ray tube. Because in space the weight and power consumption are critical parameters, we propose to use a pyroelectric X-ray generator (PXG) as a source for excitation of characteristic X-rays in sample. This type of source has already been used in energy dispersive X-ray

fluorescence instruments.^{9,10} The use of PXG for planetary XRF instrument has been studied previously with focus on source development.^{11,12} The present work uses a commercial source and is focused on the improvement of detector resolution, measurement reproducibility, and peak selection algorithm implementation.

We designed an instrument to reach a high technology maturity level based on European Space Agency (ESA) scale called Technology Readiness Level (TRL).¹³ This scale is going from level 1 (basic theoretical principle) to level 9 (space flight-proven technology). We are aiming at level of 6 (full-scale model demonstration in relevant environment) or 7 (model demonstrator for operational environment). The most difficult requirements are vacuum compatibility and radiation resistance.

The main improvements of our instrument, compared to previous work, are:

- Custom electronic readout for SDD to improve the overall resolution.
- Improvement of measurement reproducibility using PXG.
- Implementation of peak search algorithm to improve accuracy despite instrument aging.

2 | PXG AS A SOURCE OF CHOICE

PXG uses a pyroelectric crystal (LiTaO_3) to generate energetic electrons that produce X-rays in the target material. The hermetically sealed package has a thin beryllium window, which allows the X-rays to be transmitted. When heated, a pyroelectric crystal exhibits spontaneous decrease of polarization. Hence, as the temperature increases, an electric field develops across the crystal. For a specific crystal orientation, the top surface of the crystal gets positively charged and attracts electrons from the low-pressure gas in the environment. As the electrons impinge on the surface of the crystal, they produce characteristic X-rays (Ta) as well as bremsstrahlung X-rays. When the cooling phase starts, the spontaneous polarization increases, and the electrons from the top surface of the crystal are accelerated toward a Cu target, which is at ground potential. At this part of the cycle, Cu characteristic X-rays are produced, as well as bremsstrahlung X-rays. When the crystal temperature reaches its low point, the heating phase starts again. The PXG we use (Amptek COOL-X) can produce X-rays up to 35 keV.

Thanks to the previous study,⁹ we optimized the geometry to reduce X-rays flux from the PXG reaching the detector and hence improve XRF S/N ratio. We found an optimum angle of 38° between the axis of the PXG and the axis of the detector.

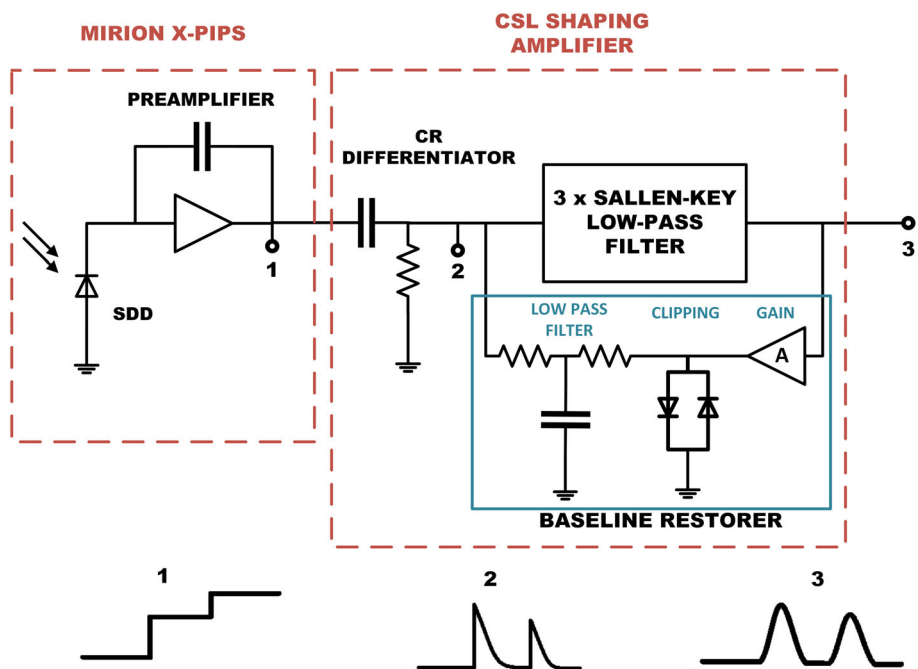
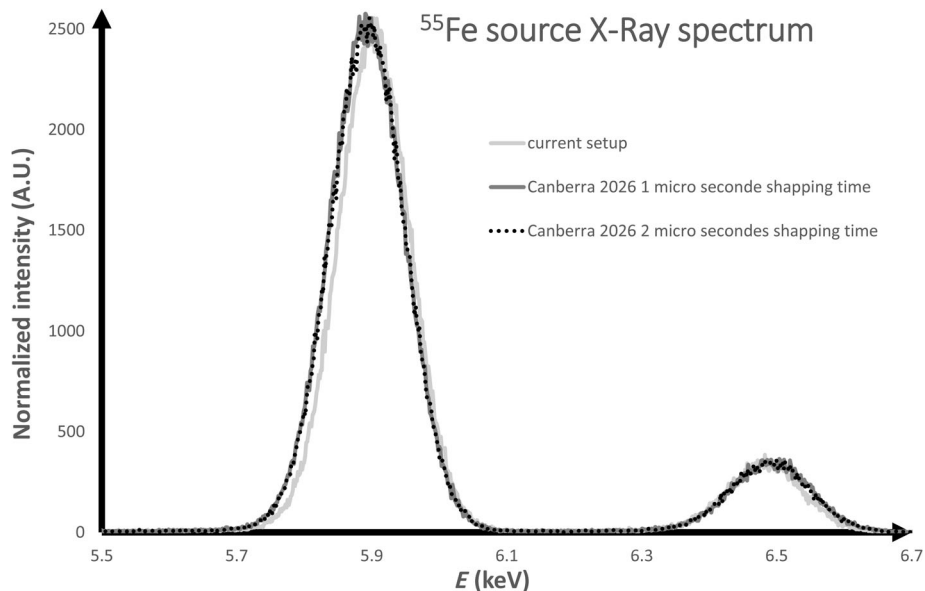
Pyroelectric sources are easier to handle (safety, regulation, and shielding) than radioisotopes and allow an easier and extensive on-ground calibration phase to study the instrument parameters on a wide range of samples. Besides, PXG should allow shorter measurement time than radioisotopes: one Amptek COOL-X is equivalent to 2 mCi source (data from manufacturer) and the geometry of our instrument allows to use 6 PXG. If we use the same geometry but with latest PXG, which is 70 times more intense than COOL-X,¹¹ we would have a source equivalent to ~ 840 mCi, 21 times the activities of the radioisotopes sources onboard APXS¹⁴ instrument on Mars.

3 | ELECTRONIC READOUT

The electronic readout is designed to meet space requirements: size reduction, weight, vacuum compatibility, and

radiation hardening. This design is also an opportunity to improve energy resolution. For a given instrument, the resolution is the quadratic sum of the resolution of its detector and the resolution of its electronic readout.¹⁵ In the previous years, there have been several improvements in detector resolution (i.e., semiconductor manufacturing¹⁶ and CMOS preamplifiers¹⁷) but less improvement came from the electronic readout. The main trend is to use digital electronics like DSP¹⁸ this is promising and will allow improvements, thanks to innovative algorithms and hardware.¹⁹ But for space, classical rad hard electronics are often preferred to reduce possible radiation-induced single event effects present in the digital electronic.²⁰ Besides, radiation-tolerant space-qualified powerful digital electronics (processor, FPGA) are very expensive. For all these reasons, we decide to design and build a classical analog electronic readout and improve its resolution. The analog electronic board of the spectrometer performs pulse shaping, thanks to a signal conditioning circuit called a shaping amplifier. Pulse shaping is the process of changing the waveform of a transmitted pulse. The purpose of the shaping amplifier is to amplify and shape the pulses coming from the SDD integrated preamplifier (Mirion X-PIPS model SXD15M-500-PA by Canberra) allowing to optimize the signal-to-noise ratio. The resulting signal is then better suited for the measurements performed by the digital acquisition system like an multichannel analyzer (MCA). The pulse shaper is able to shape short step-like voltage pulses (30 ns rise time) coming from the SDD's preamplifier into Gaussian-shaped pulses. Effectively, the output signal of the shaping amplifier is a train of Gaussian-shaped pulses with the same shaping time of 2 μs . The shaping time is the standard deviation of the Gaussian waveform, which is the width of the pulse at 0.61 times its maximum amplitude. The height of these voltage pulses is proportional to the energy of the detected photons. A diagram highlighting the different components of the shaping amplifier (noted CSL shaping amplifier in Figure 1) and its effect on the pulse signals is shown in Figure 1. To perform Gaussian shaping, the shaping amplifier uses a Gaussian filter. The Gaussian filter is realized as a seventh-order filter implemented using the combination of a C-R high-pass filter and three second-order low-pass active filters. These second-order low-pass filters are realized using the Sallen-Key topology,²¹ also called voltage-controlled voltage source (VCVS) filter. Thanks to the use of active components such as operational amplifiers, each filter yield a pair of conjugate complex poles. The C-R filter acts as a differentiator while the active filters effectively act as six integrators. The more integrator stages, the closer the output pulses will be to a true Gaussian pulse. In practice, four integration stages are sufficient.²²

FIGURE 1 Analog electronic readout

FIGURE 2 ^{55}Fe spectrum

With frequency-domain analysis, the poles of the filter can be tuned in order to obtain a very precise shaping time.²³

A recurring problem with nuclear pulse shaping is a phenomenon known as baseline drift. The C-R filter removes any DC component from the signal. As the voltage pulses are strictly positive, this will cause the signal's baseline to shift below zero volts. To counter baseline drift, a baseline restorer circuit is implemented. The baseline restorer makes use of a feedback loop design.²⁴ Inside of the feedback loop, the shaping amplifier's output voltage is amplified, clipped, and filtered, in order to

obtain a signal that is proportional to the baseline voltage.

The filtered output is then fed back to the input of the shaping amplifier chain to cancel the baseline drift.

The output of the shaping amplifier is connected to a 16,384 channels MCA Amptek MCA8000A and the final spectrum is measured on the computer connected to the MCA.

The instrument resolution has been measured using our electronic readout and compared to a reference spectroscopy amplifier (Canberra 2026) with two different shaping times. The shaping time of our readout is 2 μs .

The measured spectrum of a ^{55}Fe source (Eckert & Ziegler Model IECB15940) is shown in Figure 2. The resolution is the full width at half maximum (FWHM) of the Mn K_{α} peak at 5.89 keV of the ^{55}Fe source. The total count measured in the resolution range of the peak ($5.89 \text{ keV} - (\text{FWHM}/2)$ to $5.89 \text{ keV} + (\text{FWHM}/2)$) was 146,898 counts. During these measurements, we thermalized the SDD enclosure at 10°C . As the SDD has an onboard Peltier cooler whose hot side is connected to the enclosure, the cold side of Peltier, connected to the SDD chip, could reach -55.9°C . The measured resolution on the Mn K_{α} peak at 5.89 keV is given in Table 1.

As our instrument is using pyroelectric sources, the induced fluorescence rate is very low (<120 photons/s). Hence, our analog electronic readout has not been tested and characterized for high flux (incoming count rate). This should be done if it is used with other sources (X-ray tube, synchrotron, etc.).

4 | RENORMALIZATION

In portable XRF, excitation source fluctuations, whatever the cause, can be an issue. As we are using pulsed PXG,

TABLE 1 Measured energy resolution on ^{55}Fe source

Electronic readout	Measured resolution (eV)
This work, 2 μs shaping time	121.17
Canberra 2026 with 1 μs shaping time	127.21
Canberra 2026 with 2 μs shaping time	128.34

variation within a pulse and inter-pulses variations are problematic. The principle of these pyroelectric sources is to heat and cool a pyroelectric crystal to produce the X-ray.²⁵ One heat-cool phase duration is typically 3 min in laboratory condition. The phase's timing (pulses) can vary in different thermal conditions that can occur in space. Therefore, a process is introduced to monitor the total source emission during a measurement and normalize the measured spectrum for the total fluence of the source. The normalization factor is obtained by monitoring the fluorescence of a known reference sample in the field of view of the instrument. An Indium thin wire is used as reference to monitor the intensity of its L_{α} line at 3.28 keV. As anorthosite is representative of lunar soil, we used a pressed pellet anorthosite standard to do 10 successive measurements using simultaneously two COOL-X PXG (one unmodified and one with Mo target instead of Cu). The typical spectrum measured is shown in Figure 3. The intensity of the Ca K_{α} line at 3.69 keV of anorthosite sample was measured 10 times during 12 min. The relative standard deviation of the 10 measurements, using the two PXG sources simultaneously (one with Cu target and one with Mo target), without renormalization was 25.2% and with normalization, it was reduced to 3.71%.

5 | CALIBRATION AND PEAK SEARCH ALGORITHM

As our instrument will be used in space (i.e., Moon or Mars probe), a concern is about the peak's region of

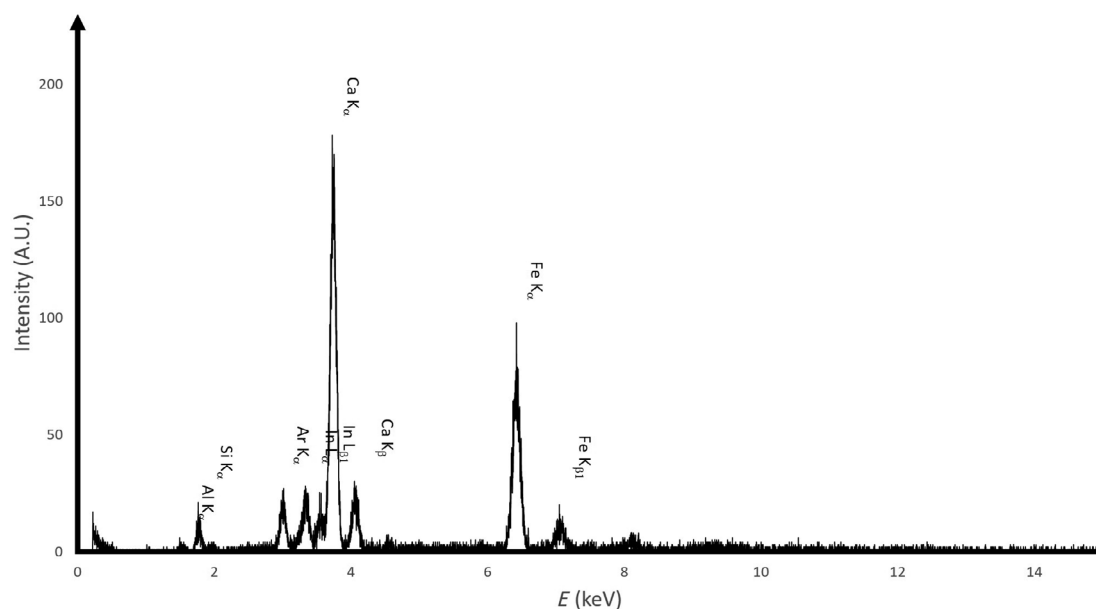


FIGURE 3 Anorthosite with in wire spectrum

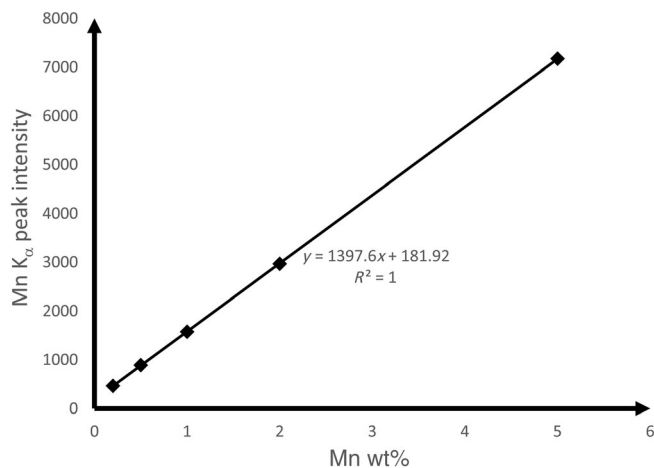


FIGURE 4 Calibration with region of interest search algorithm

interest (ROI) definitions. The ROI width can be affected by the thermal environment because temperature can affect SDD resolution.²⁶ Besides, induced space radiation aging of electronic components can also affect the position of the peak because radiation can modify the amplifiers' parameters²⁷ (i.e., gain). The peak's width of a given fluorescence line can also be modified due to radiation-induced noise in electronic.²⁸

A peak search algorithm²⁹ is used to define the best ROI for a given peak with a calibration. This could be implemented in flight with a filter wheel onboard the instrument. The wheel would have several reference samples that would be used to rerun the algorithm to optimize ROI even with aging instrument in space ionizing radiation environment. The wheel reference samples could be synthetic samples of anorthosite with increasing content of atoms of interest for lunar geology. The procedure is tested with samples of anorthosite with added amount of Mn (0.2%, 0.5%, 1%, 2%, and 5%). The algorithm is used with renormalized spectrum as explained in previous chapter. The best ROI found with the algorithm has allowed to obtain a perfect linear calibration ($r^2 = 1$) as illustrated in Figure 4. For higher concentration, a quadratic curve should be used to take into absorption or possible count reduction due to pileup.

6 | CONCLUSIONS

A TRL 6-7 model of an X-ray fluorescence spectrometer is built using pyroelectric sources that will be used for planetary probe. The achieved spectral energy resolution using a new electronic readout is 121.17 eV. The measurements repeatability, relative standard deviation, can be lowered from 25.2% to 3.71% thanks to renormalization. A dedicated algorithm is used to find

the best ROI for the fluorescence peak to compensate instrument aging in space.

An extensive test campaign should be performed with the current instrument to determine the limits of detection of the current instrument on a wide range of geological standards.

An interesting future implementation of the instrument could use the latest PXG developments¹⁰ and our detector with improved resolution, renormalization, and peak search algorithm.

ACKNOWLEDGMENT

This work is done within the ALEXIS (A Lunar Experiment of X-ray Induced Spectrometry) project funded by Belspo (Federal Public Planning Service Science Policy from Belgium) in the frame of ESA GSTP program.

DATA AVAILABILITY STATEMENT

The data that support the findings of this study are available from the corresponding author upon reasonable request.

ORCID

Alain Carapelle  <https://orcid.org/0000-0003-1947-2481>

Mathieu Morelle  <https://orcid.org/0000-0002-6299-5336>

REFERENCES

- [1] F.-P. Hocquet, H.-P. Garnir, A. Marchal, M. Clar, C. Oger, D. Strivay, *X-Ray Spectrom.* **2008**, *37*, 304.
- [2] A. Argyrakia, M. H. Ramseya, P. J. Potts, *Analyst* **1997**, *122*, 743.
- [3] R. Ravansari, S. C. Wilson, M. Tighe, *Environ. Int.* **2020**, *134*, 105250.
- [4] A. Carapelle, K. Fleury-Frenette, J.-P. Collette, H.-P. Garnir, P. Harlet, *Rev. Sci. Instrum.* **2007**, *78*, 123109.
- [5] L. Ge, F. Li, *X-Ray Spectrom.* **2020**, *49*, 458.
- [6] P. J. Potts, M. West, *Portable X-ray Fluorescence Spectrometry, Capabilities for In Situ Analysis*, RSC Publishing, Cambridge **2008**.
- [7] R. Rieder, R. Gellert, J. Brückner, G. Klingelhöfer, G. Dreibus, A. Yen, S. W. Squyres, *JGR Planets* **2003**, *108*, E12.
- [8] A. Allwood, B. Clark, D. Flannery, J. Hurowitz, L. Wade, T. Elam, M. Foote, E. Knowless, presented at IEEE Aerospace Conf, **2015**, 1–13
- [9] H. Ida, J. Kawai, *X-Ray Spectrom.* **2005**, *34*, 225.
- [10] J. Kawai, H. Ishii, H. Ida, *X-Ray Spectrom.* **2012**, *41*, 216.
- [11] H. Nagaoka, N. Hasebe, M. Naito, E. Shibamura, H. Kuno, M. Mizone, K. J. Kim, *JSASS Aerospace Tech. Japan* **2018**, *16*, 137.
- [12] H. Nagaoka, T. Okada, H. Kusano, N. Tanaka, M. Naito, N. Hasebe, *Trans. JSASS Aerospace Tech. Japan* **2021**, *19*, 193.
- [13] ESA ECSS-E-HB-11A.
- [14] T. Economou, *Radiat. Phys. Chem.* **2001**, *61*, 191.
- [15] N. Tsoufanidis, S. Landsberger, *Measurement and Detection of Radiation*, 3rd ed., Boca Raton: CRC Press, **2011**. <https://doi.org/10.1201/9781439894651>

- [16] A. Niculae, T. Barros, A. Bechteler, R. Lackner, K. Hermenau, K. Heizinger, T. Mönninghoff, H. Soltau, L. Strüder, *Microsc. Microanal.* **2019**, 25, 516.
- [17] L. Bombelli, C. Fiorini, T. Frizzi, R. Nava, A. Greppi, A. Longoni, presented at IEEE Nucl. Sci. Symp. Med. Imaging Conf, **2010**
- [18] R. P. Alvarez, P. Van Espen, J. R. E. Alvarez, *X-Ray Spectrom.* **2006**, 35, 178.
- [19] D. H. N. Quy, P. N. Tuan, N. N. Dien, *JASMI* **2019**, 9, 22.
- [20] N. Rezzak, J-J. Wang, D. Dsilva, N. Jat, IEEE Radiation Effects Data Workshop **2015**.
- [21] P. Horowitz, W. Hill, *The Art of Electronics*, 3rd ed., New-York: Cambridge University Press, **2015**.
- [22] G. F. Knoll, *Radiation Detection and Measurement*, 4th ed., John Wiley and Sons, New York **2010**.
- [23] S. Ohkawa, M. Yoshizawa, K. Husimi, *Nucl. Instrum. Methods* **1976**, 138, 85.
- [24] Q. Zhou, Z. Wang, A DC-servo baseline restorer and its implementation in biomedical instrumentation. *ICMIT Mechatronics, MEMS, and Smart Materials*. SPIE PROCEEDINGS 6040. Bellingham, Washington: SPIE; **2005**
- [25] J. D. Brownridge, S. Raboy, *J. Appl. Phys.* **1999**, 86(1), 640.
- [26] P. Lechner, C. Fiorini, R. Hartmann, J. Kemmer, N. Krause, P. Leutenegger, A. Longoni, H. Soltau, D. Stötter, R. Stötter, L. Strüder, U. Weber, *Nucl. Instrum. Methods Phys. Res. A: Accel. Spectrom. Detect. Assoc. Equip.* **2001**, 458, 281.
- [27] A. H. Johnston, B. G. Rax, D. Thorbourn, *IEEE Trans. Nucl. Sci.* **2008**, 55, 1953.
- [28] V. Re, L. Gaioni, M. Manghisoni, L. Ratti, G. Traversi, *IEEE Trans. Nucl. Sci.* **2008**, 55, 3272.
- [29] A. Carapelle, J.-M. Defise, D. Strivay, H.-P. Garnir, *Comput. Phys. Commun.* **2011**, 182, 1304.

How to cite this article: A. Carapelle, G. Lejeune, M. Morelle, O. Evrard, P. Leroux, J. Prinzie, Y. Cao, B. Van Bockel, F. Montfort, N. Martin, *X-Ray Spectrom* **2022**, 1. <https://doi.org/10.1002/xrs.3282>